Automatic Spectral Target Recognition in Hyperspectral Imagery

HSUAN REN, Member, IEEE
National Central University
Taiwan

CHEIN-I CHANG, Senior Member, IEEE
University of Maryland Baltimore County

Automatic target recognition (ATR) in hyperspectral imagery is a challenging problem due to recent advances of remote sensing instruments which have significantly improved sensor's spectral resolution. As a result, small and subtle targets can be uncovered and extracted from image scenes, which may not be identified by prior knowledge. In particular, when target size is smaller than pixel resolution, target recognition must be carried out at subpixel level. Under such circumstance, traditional spatial-based image processing techniques are generally not applicable and may not perform well if they are applied. The work presented here investigates this issue and develops spectral-based algorithms for automatic spectral target recognition (ASTR) in hyperspectral imagery with no required a priori knowledge, specifically, in reconnaissance and surveillance applications. The proposed ASTR consists of two stage processes, automatic target generation process (ATGP) followed by target classification process (TCP). The ATGP generates a set of targets from image data in an unsupervised manner which will subsequently be classified by the TCP. Depending upon how an initial target is selected in ATGP, two versions of the ASTR can be implemented, referred to as desired target detection and classification algorithm (DTDCA) and automatic target detection and classification algorithm (ATDCA). The former can be used to search for a specific target in unknown scenes while the latter can be used to detect anomalies in blind environments. In order to evaluate their performance, a comparative and quantitative study using real hyperspectral images is conducted for analysis.

Manuscript received August 10, 2001; revised December 10, 2002; released for publication October 4, 2003.

IEEE Log No. T-AES/39/4/821711.

Refereeing of this contribution was handled by J. Barnett.

The work of C.-I Chang was supported by Bechtel Nevada Corporation, DE-AC08-96NV11718 through the Department of Energy and Office of Naval Research, N00014-01-1-0359.

Authors' addresses: H. Ren, Center for Space and Remote Sensing Research, Dept. of Information Engineering, National Central University, Chungli, Taiwan; C.-I Chang, Remote Sensing Signal and Image Processing Laboratory, Dept. of Computer Science and Electrical Engineering, University of Maryland Baltimore County, Baltimore, MD 21250.

I. INTRODUCTION

Hyperspectral imaging is an emerging technique due to recent advances of remote sensing instruments, e.g., imaging spectrometers. Two currently in use and operated in airborne platform are the NASA Jet Propulsion Laboratory's Airborne Visible/InfraRed Imaging Spectrometer (AVIRIS) and the Naval Research Laboratory's HYperspectral Digital Imagery Collection Experiment (HYDICE) sensor and many more are yet to be developed. These sensors can be used in a broad range of applications ranging from geology, agriculture, and global change to defense, intelligence, and law enforcement. One main advantage of hyperspectral sensor technology is the significantly improved spectral and spatial resolutions so that many subtle material substances which cannot be resolved by multispectral sensors such as SPOT (Satellite Pour l'Observation de la Terra) and LANDSAT can be now diagnosed by as many as 200 contiguous 10 nm wide spectral bands used in hyperspectral sensors. However, this also comes at a price that many unknown signal sources may be also uncovered as anomalies without prior knowledge. This is particularly true when targets with size smaller than pixel resolution such as small man-made targets are actually embedded in a single pixel. In order to detect these targets, one must rely on their spectral properties to extract them at a subpixel scale, a task which cannot be accomplished by traditional spatial-based image processing techniques. Therefore, one of the major challenges for hyperspectral imaging has been automatic spectral target recognition (ASTR) in hyperspectral images as opposed to automatic spatial target recognition, commonly referred to as automatic target recognition (ATR) in the literature. Most distinctively, a hyperspectral image is actually an image cube with the third dimension is specified by spectral wavelengths. Consequently, a hyperspectral image pixel is indeed a column vector.

ASTR in an unknown image background can be difficult. An early attempt was made to use an unsupervised vector quantization-based clustering method to find a number of clusters where each of the cluster centers corresponds to one potential target [1]. This approach, however, requires the prior knowledge of the number of clusters, which is a well-known problem in unsupervised classification [2]. A similar problem also arises in sensor array processing where the number of signals must be known a priori or estimated by an information theoretic criterion (Akaike information criterion) [3–4] or minimum description length (MDL) [4–5]. However, AIC or MDL may not be appropriate to be used to determine the number of targets present in remotely sensed images as shown in [6]. This is because the noise in remotely sensed imagery may not be stationary and not even be independent identically distributed.

Secondly, the data statistics may not be available or may be difficult to obtain in order to implement the likelihood functions used in these criteria.

This paper investigates the issue of the ASTR and develops algorithms for the ASTR in hyperspectral imagery. The proposed ASTR algorithms can be implemented by an automatic target generation process (ATGP) followed by a target classification process (TCP). The ATGP generates a set of potential targets from the image data in an unsupervised fashion without any prior knowledge. Then the resulting ATGP-generated targets are subsequently classified by the TCP. The idea of the ATGP originates from the concept of orthogonal subspace projection (OSP) in signal processing, which was previously used to develop an OSP classifier for hyperspectral image classification [7]. The ATGP first selects an initial target pixel vector, denoted by $\mathbf{t}_0$, then uses the OSP to project all image pixel vectors into the orthogonal complement space of the linear space spanned by $\mathbf{t}_0$, denoted by $\langle \mathbf{t}_0 \rangle^{\perp}$ that is orthogonal to $\mathbf{t}_0$. A pixel vector with the maximum length in $\langle \mathbf{t}_0 \rangle^{\perp}$ is then selected as a first target pixel vector extracted from the data, denoted by $\mathbf{t}_1$. Since $\mathbf{t}_1$ produces the maximum magnitude of projection in $\langle \mathbf{t}_0 \rangle^{\perp}$, we can expect that these two target pixel vectors $\mathbf{t}_0$ and $\mathbf{t}_1$ have most distinct spectral features in the sense of orthogonal projection. The same procedure is repeated again to generate a second target pixel vector $\mathbf{t}_2$, a third target pixel vector $\mathbf{t}_3$, etc. until a stopping criterion is met. In this case, the ATGP is terminated. Next, the targets produced by the ATGP are processed by the TCP which classifies each of the ATGP-generated targets. The classifier used in the TCP is the OSP classifier developed in [7]. The reason for this selection is because both the ATGP and the TCP use the OSP as a criterion to generate and classify targets. Nevertheless, it by no means claims that the OSP classifier is the best classifier. Other classifiers can be also used in the TCP in accordance with different applications.

It should be noted that there is a difference between the initial target pixel vector $\mathbf{t}_0$ and other target pixel vectors $\mathbf{t}_j$ for $j \neq 0$ generated in the ATGP. While $\mathbf{t}_0$ could be selected with some judicious reasoning, $\mathbf{t}_j$ can only be generated by the OSP. As a result, depending upon how the initial target pixel vector $\mathbf{t}_0$ is selected in the ATGP, two versions of the ASTR can be designed for different applications. If the initial target $\mathbf{t}_0$ is selected by a priori knowledge, the ASTR algorithm is referred to as desired target detection and classification algorithm (DTDCA). In this case, DTDCA can be used to search for a specific target in unknown scenes. It is often the case that in reconnaissance applications the targets of interest are generally provided by prior knowledge. Therefore, they can all be used as initial target pixel vectors, not necessarily a single initial target pixel vector. The DTDCA allows one to detect all such target pixel vectors in the image data. On the other hand, if the initial target is not specified and provided a priori, it must be generated by the ATGP. To meet this need an automatic detection and classification algorithm (ATDCA) is developed. In this case, the ATDCA can be used to detect anomalies in completely blind and unknown environments. This situation occurs in surveillance applications when no prior knowledge is available, e.g., concealed target detection, environmental monitoring, etc. Despite that the only difference between the DTDCA and the ATDCA lies in the selection of the initial target pixel vector $\mathbf{t}_0$, it results in different applications as demonstrated in experiments conducted here. For the DTDCA it only classifies the target pixel vectors specified by $\mathbf{t}_0$ and only these target pixel vectors are shown in the classification images. By contrast, the ATDCA classifies all the target pixel vectors specified by the target pixel vectors generated by the ATGP. As a result, each ATGP-generated target yields an individual and separate classification image.

Several advantages can be benefited from the ASTR. 1) The targets produced by the ATGP may include interferers such as clutter and also natural background signatures which cannot be identified from image data a priori. They can be eliminated to improve target detection performance. This is specially crucial for hyperspectral images where interference tends to have more dominant impacts than noise on detection and classification [8]. As a consequence, interference elimination and suppression is more important than noise removal. However, interference is generally difficult to identify in the image data. The ATGP provides a feasible means for finding such interferers. 2) Unless a complete target knowledge is available a priori, the ASTR provides a mechanism to find unknown targets and interferers. The ASTR makes use of the ATGP to generate such potential targets without appealing for prior knowledge. 3) The ASTR extends existing classifiers such as OSP classifier in [7], signature subspace classifier (SSC), oblique subspace classifier (OBC) in [9], maximum likelihood classifier (MLC) [10–11] and Kalman filter-based classifier [12] in an unsupervised fashion. Moreover, it can be further used to detect anomalous or concealed targets [13]. In order to evaluate both ASTR algorithms, the DTDCA and the ATDCA, a comparative and quantitative study is conducted using a series of experiments using HYDICE data to demonstrate their difference and performance analysis.

This paper is organized as follows. Section II formulates hyperspectral image mixed pixel classification as a linear mixing problem where the OSP approach developed in [7] is also reviewed. Section III develops the ASTR that comprises two processes, the ATGP and the TCP implemented in sequence. Two versions of the ASTR, DTDCA, and ATDCA are also described in the section. Section

IV presents a series of experiments using HYDICE image data to demonstrate the difference between the DTDCA and the ATDCA. In particular, a quantitative study and comparative analysis is conducted for their performance evaluation. Section V concludes a general discussion on the ASTR and its applications.

II. ORTHOGONAL SUBSPACE PROJECTION

Linear spectral mixing analysis is a classic approach in remote sensing image processing to determine and quantify individual spectral signatures (or endmembers) in a mixed pixel [14–15]. Many other approaches were also developed for hyperspectral image analysis [16]. Of particular interest is the OSP approach in [7–9, 17] which has shown success and been widely used in hyperspectral and multispectral data exploitation. It is also based on a linear mixture model, but takes a slightly different view from commonly used linear unmixing methods such as maximum likelihood estimation [10–11]. It separates the undesired targets from the desired target in the mixture model, then utilizes an orthogonal subspace projector to eliminate the undesired targets prior to detection and classification. Unfortunately, the OSP approach cannot be used for ATR since it requires complete target knowledge. In many practical and real applications, such prior knowledge is either not available or difficult to obtain. Under such circumstance, the required knowledge must be generated directly from the image data in an unsupervised means. This is particularly important for reconnaissance and surveillance applications where the image environment is generally unknown. The proposed ASTR is designed and developed based on this need. It extends the OSP approach to ATR in two different aspects which result in two different algorithms, DTDCA and ATDCA. As mentioned previously, the OSP approach is a spectral-based technique and we use the term ASTR in this work instead of the commonly used ATR to make such a distinction.

A. Linear Mixing Problems

In order to describe the OSP approach, we first review a linear mixing problem. Suppose that L is the number of spectral bands and there are p target signatures, $\mathbf{m}_1,\mathbf{m}_2,\ldots,\mathbf{m}_p$ present in the image with $\mathbf{m}_j$ being an $L\times 1$ column vector represented by the jth target signature. Let $\mathbf{r}$ be an $L\times 1$ column vector and denote the spectral signature of an image pixel vector in a hyperspectral image. A linear mixing problem assumes that the spectral signature $\mathbf{r}$ is a linear mixture of the p target signatures, $\mathbf{m}_1,\mathbf{m}_2,\ldots,\mathbf{m}_p$; then finds their corresponding abundance fractions, denoted by $\alpha_1,\alpha_2,\ldots,\alpha_p$ where α_j denotes the fraction of the jth target signature $\mathbf{m}_j$ resident in pixel vector $\mathbf{r}$. More precisely, let $\mathbf{M}=[\mathbf{m}_1\ \mathbf{m}_2\cdots\mathbf{m}_p]$ be an $L\times p$ target signature matrix formed from the p target signatures $\mathbf{m}_1,\mathbf{m}_2,\ldots,\mathbf{m}_p$ and α be a $p\times 1$ abundance column vector denoted by $(\alpha_1\ \alpha_2\cdots\alpha_p)^T$ corresponding to $\mathbf{m}_1,\mathbf{m}_2,\ldots,\mathbf{m}_p$. A linear mixture model for $\mathbf{r}$ is described by

$$\mathbf{r}=\mathbf{M}\alpha+\mathbf{n} \tag{1}$$

where $\mathbf{n}$ is an $L\times 1$ column vector representing additive white noise with zero mean and variance $\sigma^2\mathbf{I}_{L\times L}$ and $\mathbf{I}_{L\times L}$ is the $L\times L$ identity matrix. A linear mixing problem is to solve a linear inverse problem of (1) by finding an appropriate α that represents true abundance fractions of each of $\mathbf{m}_1,\mathbf{m}_2,\ldots,\mathbf{m}_p$ present in the $\mathbf{r}$. So, a remotely sensed image pixel vector is generally a mixed pixel whose signature is a mixture of target signatures such as the one formed by (1). For example, if the $\mathbf{r}$ contains only one target signature, the abundance of this particular target signature will be 100% and the rest of them will be zero. In this case, the corresponding pixel vector is reduced to a scalar pure pixel which is the case considered in traditional image processing.

B. Orthogonal Subspace Projection

First of all, we rewrite model (1) as follows

$$\mathbf{r}=\mathbf{t}\alpha_p+\mathbf{U}\gamma+\mathbf{n} \tag{2}$$

where $\mathbf{t}=\mathbf{m}_p$ is assumed to be a desired target signature and $\mathbf{U}=[\mathbf{m}_1\ \mathbf{m}_2\cdots\mathbf{m}_{p-1}]$ is the undesired spectral signature matrix made up of a set of the remaining $p-1$ undesired target signatures. Here, we assume without loss of generality that the last target signature is the desired target signature $\mathbf{t}$. Nevertheless, (2) can be extended straightforwardly to more than one desired target signature. Separating $\mathbf{U}$ from $\mathbf{M}$ allows us to design an orthogonal subspace projector to annihilate $\mathbf{U}$ from an image pixel vector prior to detection and classification. One such projector was an undesired target signature annihilator developed in [7] and given by

$$P_{\mathbf{U}}^{\perp}=\mathbf{I}-\mathbf{U}\mathbf{U}^{\#} \tag{3}$$

where $\mathbf{U}^{\#}=(\mathbf{U}^T\mathbf{U})^{-1}\mathbf{U}^T$ is the pseudoinverse of $\mathbf{U}$ and the notation $^{\perp}_{\mathbf{U}}$ in $P_{\mathbf{U}}^{\perp}$ indicates that the projector $P_{\mathbf{U}}^{\perp}$ maps the observed pixel $\mathbf{r}$ into the range $\langle\mathbf{U}\rangle^{\perp}$, the orthogonal complement of $\langle\mathbf{U}\rangle$. Applying $P_{\mathbf{U}}^{\perp}$ to model (2) results in a new model

$$P_{\mathbf{U}}^{\perp}\mathbf{r}=P_{\mathbf{U}}^{\perp}\mathbf{t}\alpha_p+P_{\mathbf{U}}^{\perp}\mathbf{n} \tag{4}$$

where the undesired target signatures in $\mathbf{U}$ have been eliminated and the original noise $\mathbf{n}$ has been suppressed to $P_{\mathbf{U}}^{\perp}\mathbf{n}$.

Equation (4) represents a standard signal detection problem. Operating a pixel vector $\mathbf{x}$ on (4) and

choosing maximization of the signal-to-noise ratio (SNR) given by

$$\mathrm{SNR}(\mathbf{x}) = \frac{(\mathbf{x}^T P_{\mathbf{U}}^{\perp}\mathbf{t})\alpha_p^2(\mathbf{t}^T P_{\mathbf{U}}^{\perp}\mathbf{x})}{\mathbf{x}^T P_{\mathbf{U}}^{\perp} E[\mathbf{n}\mathbf{n}^T] P_{\mathbf{U}}^{\perp}\mathbf{x}} \tag{5}$$

as the optimal criterion, the maximum SNR of (5) can be obtained by a matched filter, denoted by $\mathbf{M}_{\mathbf{t}}$ with $\mathbf{x} = \kappa\mathbf{t}$ where κ is a constant and the desired matched signal happens to be the desired target signature $\mathbf{t}$.

Based on the approach outlined by (2)–(5), the OSP approach is carried out by a two-stage process, i.e., an undesired target signature annihilator $P_{\mathbf{U}}^{\perp}$ followed by a matched filter $\mathbf{M}_{\mathbf{t}}$. More precisely, if we want to classify a desired target signature $\mathbf{t}$ in the $\mathbf{r}$ based on model (1), we first apply $P_{\mathbf{U}}^{\perp}$ to model (2) to eliminate $\mathbf{U}$, then use the matched filter $\mathbf{M}_{\mathbf{t}}$ to extract $\mathbf{t}$ from the signal detection model (4). The operator coupling $P_{\mathbf{U}}^{\perp}$ with $\mathbf{M}_{\mathbf{t}}$ is called an orthogonal subspace classifier, P_{OSP} in [7] and denoted by

$$P_{\mathrm{OSP}} = \mathbf{M}_{\mathbf{t}} P_{\mathbf{U}}^{\perp} = \mathbf{t}^T P_{\mathbf{U}}^{\perp}. \tag{6}$$

III. AUTOMATIC TARGET RECOGNITION (ATR) ALGORITHM

As shown in (6), P_{OSP} requires the complete knowledge of the desired target signature $\mathbf{t}$ and the undesired target signatures in $\mathbf{U}$. In many practical applications, it is difficult to specify $\mathbf{U}$. In this section, we present an OSP-based ASTR approach which does not require the prior knowledge about target signatures in $\mathbf{U}$. It comprises two processes, ATGP followed by TCP.

Assume that $\mathbf{t}_0$ is an initial target signature. The ATGP begins with the initial target signature $\mathbf{t}_0$ by applying an orthogonal subspace projector $P_{\mathbf{t}_0}^{\perp}$ to all image pixel vectors and finds a target signature, denoted by $\mathbf{t}_1$ with the maximum orthogonal projection in the orthogonal complement space, denoted by $\langle \mathbf{t}_0 \rangle^{\perp}$ that is orthogonal to the space $\langle \mathbf{t}_0 \rangle$ linearly spanned by $\mathbf{t}_0$. The reason for this selection is that the selected $\mathbf{t}_1$ generally has the most distinct features from $\mathbf{t}_0$ in the sense of orthogonal projection because $\mathbf{t}_1$ has the largest magnitude of the projection in $\langle \mathbf{t}_0 \rangle^{\perp}$ produced by $P_{\mathbf{t}_0}^{\perp}$. A second target signature $\mathbf{t}_2$ can be found by applying an orthogonal subspace projector $P_{[\mathbf{t}_0\mathbf{t}_1]}^{\perp}$ to the original image and a target signature that has the maximum orthogonal projection in $\langle \mathbf{t}_0, \mathbf{t}_1 \rangle^{\perp}$ is selected as $\mathbf{t}_2$. The above procedure is repeated again to find a third target signature $\mathbf{t}_3$, a fourth target signature $\mathbf{t}_4$, etc. In order to terminate the ATGP a stopping rule is required. If we let $\mathbf{U}_i = [\mathbf{t}_1\ \mathbf{t}_2 \cdots \mathbf{t}_i]$ be the ith target signature matrix generated at the ith stage, we define an orthogonal projection correlation index (OPCI) by

$$\eta_i = \mathbf{t}_0^T P_{\mathbf{U}_i}^{\perp} \mathbf{t}_0 \tag{7}$$

which can be used to measure the similarity between two consecutive generated target signatures. Since $\mathbf{U}_{i-1} \subset \mathbf{U}_i$, $\eta_i = \mathbf{t}_0^T P_{\mathbf{U}_i}^{\perp}\mathbf{t}_0 \le \eta_{i-1} = \mathbf{t}_0^T P_{\mathbf{U}_{i-1}}^{\perp}\mathbf{t}_0$ for all is. This implies that the sequence $\{\mathbf{t}_0^T P_{\mathbf{U}_i}^{\perp}\mathbf{t}_0\}$ is monotonically decreasing at i. In other words, the OPCI sequence $\{\eta_i\}$ is monotonically decreasing at i. Using this property as a stopping criterion, the ATGP can be summarized as follows.

Automatic Target Generation Process:

1) Initial condition:
   Select an initial target signature of interest denoted by $\mathbf{t}_0$. Let ε be the prescribed error threshold. Set $i = 0$ and $\mathbf{U}_0 = \phi$.
2) Apply $P_{\mathbf{t}_0}^{\perp}$ via (3) to all image pixel vectors $\mathbf{r}$ in the image.
3) Find the first target signature, denoted by $\mathbf{t}_1$ which has the maximum orthogonal projection
$$\mathbf{t}_1 = \arg\left\{\max_{\mathbf{r}}[(P_{\mathbf{t}_0}^{\perp}\mathbf{r})^T(P_{\mathbf{t}_0}^{\perp}\mathbf{r})]\right\}. \tag{8}$$
   Set $i = 1$ and $\mathbf{U}_1 = \mathbf{t}_1$.
4) If $\eta_1 = \mathbf{t}_0^T P_{\mathbf{U}_1}^{\perp}\mathbf{t}_0 < \varepsilon$, go to step 8. Otherwise, set $i = i + 1$ and continue.
5) Find the ith target $\mathbf{t}_i$ generated at the ith stage by
$$\mathbf{t}_i = \arg\left\{\max_{\mathbf{r}}[(P_{[\mathbf{t}_0\mathbf{U}_{i-1}]}^{\perp}\mathbf{r})^T(P_{[\mathbf{t}_0\mathbf{U}_{i-1}]}^{\perp}\mathbf{r})]\right\} \tag{9}$$
   where $\mathbf{U}_{i-1} = [\mathbf{t}_1\ \mathbf{t}_2 \cdots \mathbf{t}_{i-1}]$ is the target signature matrix generated at the $(i-1)$st stage.
6) Let $\mathbf{U}_i = [\mathbf{t}_1\ \mathbf{t}_2 \cdots \mathbf{t}_i]$ be the ith target signature matrix, calculate OPCI, $\eta_i = \mathbf{t}_0^T P_{\mathbf{U}_i}^{\perp}\mathbf{t}_0$ and compare η_i to a prescribed threshold ε.
7) Stopping rule: If $\eta_i > \varepsilon$, go to step 5. Otherwise, continue.
8) At this stage, the ATGP is terminated. At this point, the target matrix $\mathbf{U}_i$ generated at this point contains i target signatures which does not include the initial target signature $\mathbf{t}_0$.

After the ATGP is terminated, the ATGP-generated targets are then fed to the TCP which is used for target classification. Depending upon whether or not partial knowledge is used to select the initial target $\mathbf{t}_0$ in the ATGP two versions of the ASTR can be implemented, referred to as DTDCA and ATDCA.

A. Desired Target Detection and Classification

On many occasions, some partial knowledge may be available and can be useful. In reconnaissance applications, it is often the case that some specific targets are of interest and this knowledge should be included in algorithm design. For simplicity, we assume that there is one specific target of interest. In this case, we should take advantage of this information by selecting it as initial target $\mathbf{t}_0$. Such target can be either directly extracted from the image

scene or obtained from a spectral library. However, other than $\mathbf{t}_0$ no prior knowledge is required. The DTDCA is designed to detect and classify such a specific target $\mathbf{t}_0$ and can be implemented as follows.

Desired Target Detection and Classification Algorithm:

1) The initial target signature $\mathbf{t}_0$ is selected by a specific target of interest.
2) Use $\mathbf{t}_0$ as the initial target signature in the ATGP to generate a set of targets signatures to form $\mathbf{U}_i$.
3) Use the TCP to classify $\mathbf{t}_0$:
   It should be noted that when we classify the target signature $\mathbf{t}_0$, any target signature in $\mathbf{U}_i$ generated by the ATGP will be considered as an undesired target signature with respect to $\mathbf{t}_0$ no matter what this target signature is. In this case, the generated target matrix $\mathbf{U}_i$ will substitute for the $\mathbf{U}$ in (2) to yield the desired OSP classifier given by $P_{\text{OSP}} = \mathbf{t}_0^T P_{\mathbf{U}_i}^{\perp}$. The resulting image will detect and classify all target pixels specified by $\mathbf{t}_0$.

B. Automatic Target Detection and Classification Algorithm

Unlike the DTDCA where the initial target in the ATGP was assumed to be known a priori, the ATDCA assumes no prior knowledge including $\mathbf{t}_0$. In this case, the ATGP must be implemented in an unsupervised fashion. In order to initialize the ATGP without knowing $\mathbf{t}_0$, we select a target signature with the maximum length as the initial target $\mathbf{t}_0$, namely, $\mathbf{t}_0 = \arg\{\max_{\mathbf{r}}[\mathbf{r}^T\mathbf{r}]\}$. The $\mathbf{t}_0$ resulting from this selection may not necessarily be a target signature. It could be an interfering signature, a background signature or something which is not of interest. Since no prior knowledge is available, we must classify the $\mathbf{t}_0$ and all other targets generated by the ATGP in $\mathbf{U}_i$ individually and separately. This is a subtle but crucial difference between the DTDCA and the ATDCA, which also results in different applications.

A detailed implementation of the ATDCA is given as follows.

Automatic Target Detection and Classification Algorithm:

1) Select $\mathbf{t}_0 = \arg\{\max_{\mathbf{r}}[\mathbf{r}^T\mathbf{r}]\}$.
2) Use $\mathbf{t}_0$ as the initial target signature in step 1 of the ATGP.
3) Follow steps 2–8 outlined in the ATGP to generate $\mathbf{U}_i$.
4) Use the TCP to classify $\mathbf{t}_0$ and all the targets in $\mathbf{U}_i$ individually.
   Apply the OSP classifier $P_{\text{OSP}} = \mathbf{t}_j^T P_{\mathbf{U}}^{\perp}$ to classify all individual targets $\mathbf{t}_j$ with $\mathbf{U} = [\mathbf{t}_0\ \mathbf{t}_1 \cdots \mathbf{t}_{j-1}\ \mathbf{t}_{j+1} \cdots \mathbf{t}_i]$. Since there are $i+1$ target signatures (i.e., $\mathbf{t}_0$ and i target signatures $\mathbf{t}_1, \mathbf{t}_2, \ldots, \mathbf{t}_i$ in $\mathbf{U}_i$), $i+1$ images will be generated by the TCP, each of which detects and classifies one particular target.

C. Comments on ASTR

Five comments are noteworthy.

1) It should be noted that each cycle from step 5 to step 7 in the ATGP generates one target at a time.

2) Despite the fact that the OSP classifier is suggested to be used in the TCP in both the DTDCA and the ATDCA, other classifiers such as a posteriori OSP classifiers (SSC, OBC, MLC) [9] or Kalman-filtering-based classifier [12] can be also used to replace the OSP classifier in the TCP to meet different purposes. However, when the OSP classifier is used in the TCP, the ATR algorithm can be viewed as an extension of the OSP classifier to an unsupervised OSP classifier.

3) The criterion OPCI η_i given by (7) is particularly designed for a stopping rule. It measures how much of the residual of the orthogonal projection of the undesired signatures in $\mathbf{U}_i$ leaked into the initial target $\mathbf{t}_0$. It provides an important indication about how many targets are needed to generate for the TCP in classification. Another criterion can also be used is the differential OPCI (DOPCI) defined by $d\eta_i = \eta_{i-1} - \eta_i$ which measures the discrepancy between two consecutive OPCIs. If $d\eta(\mathbf{U}_{i-1}, \mathbf{U}_i)$ is small, it means that the currently generated target has very similar signature to previously generated targets in the sense of orthogonal projection. In this case, the new target does not make too much projection contribution to the OPCI which results in a small DOPCI. On the other hand, if η_i is small, it implies that the $\mathbf{U}_i$ generated contains by far the most significant targets in the image. In this case, it indicates that the number of targets produced by the ATGP is sufficient to warrant good classification results. However, we may use both indices as stopping rules to further ensure that 1) the number of targets is sufficient because of $\eta_i < \varepsilon_1$, and 2) no significant targets are left out because of $d\eta(\mathbf{U}_{i-1}, \mathbf{U}_i) = \eta_{i-1} - \eta_i < \varepsilon_2$ as long as thresholds ε_1 and ε_2 are sufficiently small. It should be noted that the choice of epsilons is rather empirical, generally less than 0.01. Alternatively, instead of using epsilons in the DTDCA and the ATDCA as a stopping rule we can terminate the algorithms by setting an upper bound on the number of targets needed to be generated. In this case, this upper bound must be determined in advance.

4) The initial target signature $\mathbf{t}_0$ used in the DTDCA is not necessarily limited to one single target. If there are more than one target of interest, they can all be used for initial targets. These multiple targets are then further classified individually thereafter. The algorithm using multiple targets will be expected to be terminated faster than using a single target. But this

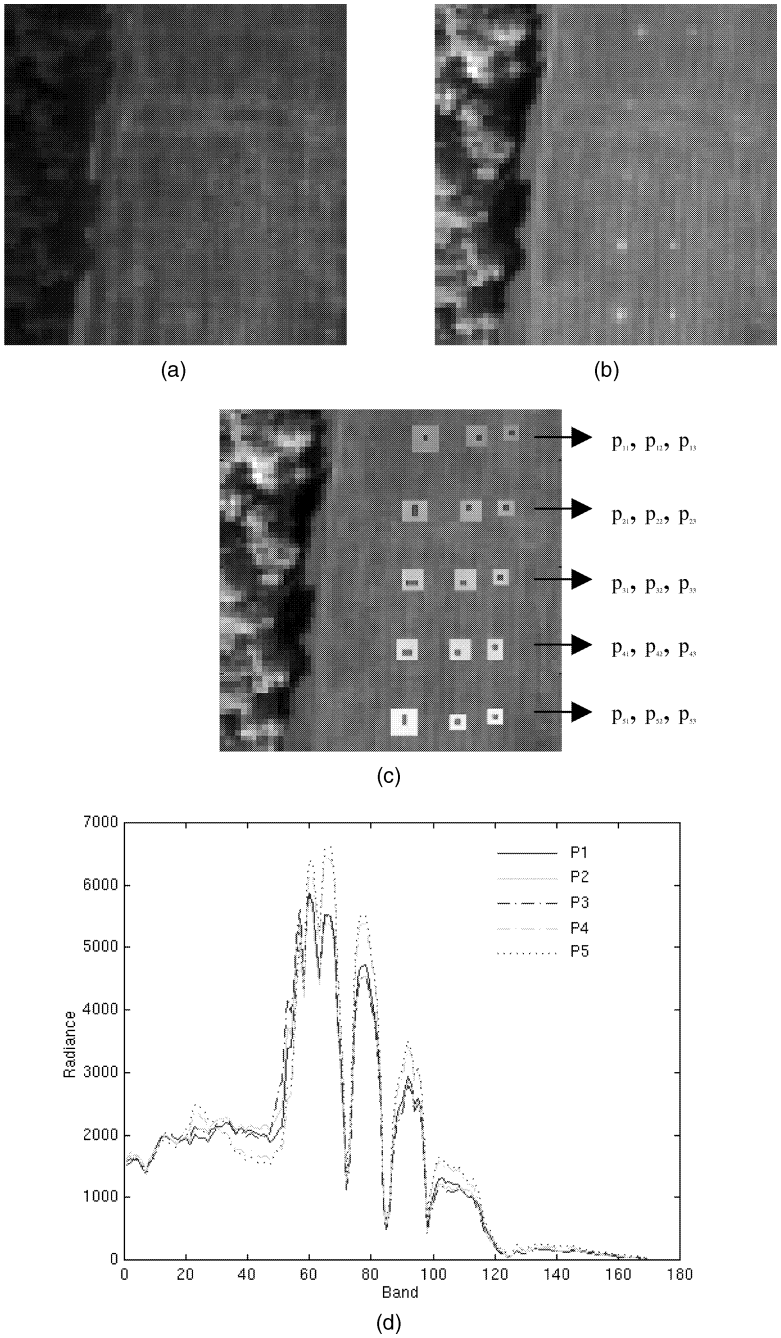

Fig. 1. (a) Band 30 HYDICE panel scene which shows no sign of 15 panels. (b) Band 80 HYDICE panel scene which contains 15 panels. (c) Ground truth map of spatial locations of 15 panels. (d) Spectra of P1, P2, P3, P4, and P5 generated from Fig. (a).

is also traded for more information required to know about the multiple targets.

5) It may be worthwhile to reiterate two subtle differences in implementation of the DTDCA and the ATDCA. One difference is the selection of the initial target signature $\mathbf{t}_0$ used in the ATGP. The DTDCA requires the knowledge of $\mathbf{t}_0$ while the ATDCA does not. So, the DTDCA can be considered to be partially supervised as opposed to the ATDCA which is completely unsupervised. The second difference is the target classification implemented in the TCP. The DTDCA only classifies the initial target signature $\mathbf{t}_0$ which is assumed to be the desired target. By contrast, the ATDCA must classify all targets generated by the ATGP since we do not know which targets are desired or undesired. As a result of these differences, the DTDCA and the ATDCA can be used for different applications.

6) It should be noted that the proposed ASTR requires no optimization method. Consequently, there is no issue of local or global optima. In addition, the computational complexity is very fast. For example, an OSP classifier is an operator implemented by an orthogonal projector $P_{\mathbf{U}}^{\perp}$ followed by a matched

filter. Both operations are simple and computationally efficient.

IV. EXPERIMENTS

In this section, a quantitative study and comparative analysis for the DTDCA and the ATDCA is conducted by a series of experiments using two HYDICE image scenes with size of 64×64 pixels where the low signal/high noise bands: bands 1–3 and bands 202–210; and water vapor absorption bands: bands 101–112 and bands 137–153 have been removed. Additionally, their difference is also demonstrated. The first HYDICE scene to be studied has 15 panels located in the center of the scene. Two bands of the same scene in Figs. 1(a)–1(b) show that the information provided by a band varies with its spectral coverage interval. Fig. 1(a) is band 30 which shows no sign of the presence of these 15 panels in the scene compared to band 80 in Fig. 1(b) where the panels are clearly visible in the scene. These 15 panels are arranged in a 5×3 matrix. Each element in this matrix is a square panel and denoted by p_{ij} with row indexed by $i = 1,\ldots,5$ and column indexed by $j = a,b,c$. For each row $i = 1,\ldots,5$, the three panels $\mathrm{p}_{ia},\mathrm{p}_{ib},\mathrm{p}_{ic}$ were painted by the same material but have three different sizes. For each column $j = a,b,c$, the five panels $\mathrm{p}_{1j},\mathrm{p}_{2j},\mathrm{p}_{3j},\mathrm{p}_{4j},\mathrm{p}_{5j}$ have the same size but were painted by five different materials. The sizes of the panels in the first, second, and third columns are $3\ \mathrm{m} \times 3\ \mathrm{m}$, $2\ \mathrm{m} \times 2\ \mathrm{m}$, and $1\ \mathrm{m} \times 1\ \mathrm{m}$, respectively. So, the 15 panels have five different materials and three different sizes. The ground truth map provided in Fig. 1(c) shows the precise spatial locations of these 15 panels. Black (B) pixels in Fig. 1(c) are the panel center pixels of all the 15 panels and white (W) pixels are panel pixels mixed with background pixels which can be considered as mixed pixels. Fig. 1(d) plots the spectra of 5 panel signatures, $\{\mathbf{s}_i\}_{i=1}^{5}$ generated by averaging B pixels in each row. The 1.5 m spatial resolution of the image scene suggests that except for $\mathrm{p}_{2a},\mathrm{p}_{3a},\mathrm{p}_{4a},\mathrm{p}_{5a}$ which are two-pixel panels, all the remaining panels are single-pixel panels.

Two sets of experiments were conducted to illustrate the difference between the DTDCA and the ATDCA and their performance.

A. Experiments for DTDCA

The first set of experiments assumed that the panel signatures in row 1 were known and given by $\mathbf{s}_1$ in Fig. 1(d). In this case, $\mathbf{t}_0 = \mathbf{s}_1$ and we applied $P_{\mathbf{t}_0}^{\perp}$ to project all image pixel vectors to the space, $\langle \mathbf{t}_0 \rangle^{\perp}$ that is orthogonal to the space linearly spanned by $\mathbf{t}_0$. Then the pixel vector in $\langle \mathbf{t}_0 \rangle^{\perp}$ with the maximum length was selected as a first target with its signature specified by $\mathbf{t}_1$. Now the OSP classifier $P_{\mathrm{OSP}} = \mathbf{t}_0^T P_{\mathbf{U}_1}^{\perp}$ was applied to the image with $\mathbf{U}_1 = \mathbf{t}_1$ as the undesired signature for elimination. The resulting image is shown in Fig. 2(a) where the corresponding OPCI $\eta_1 = 0.08147$ is shown underneath the image. As we can see, none of the panels in row 1 were detected. So, the orthogonal projector $P_{[\mathbf{t}_0\mathbf{t}_1]}^{\perp}$ was applied to the original image to find a pixel vector with the maximum length in the space $\langle \mathbf{t}_0, \mathbf{t}_1 \rangle^{\perp}$ which was selected as a second target with its signature specified by $\mathbf{t}_2$. The OSP classifier $P_{\mathrm{OSP}} = \mathbf{t}_0^T P_{\mathbf{U}_2}^{\perp}$ with $\mathbf{U}_2 = [\mathbf{t}_1\mathbf{t}_2]$ was further applied to the image scene again where the undesired target signatures $\mathbf{t}_1$, $\mathbf{t}_2$ were eliminated by orthogonal projection. The resulting image is shown in Fig. 2(b) with the corresponding OPCI $\eta_2 = 0.03742$. The same procedure was repeated over and over again to find a third target with its signature specified by $\mathbf{t}_3$, a fourth target with its signature specified by $\mathbf{t}_4$, etc. Fig. 2 shows that a total of 20 undesired target signatures was generated by the ATGP for elimination in sequence to classify the desired target signature $\mathbf{t}_0 = \mathbf{s}_1$. Five stages in the detection process were interesting and worth mentioning. The first stage is demonstrated by Figs. 2(a)–2(c) where no panels were detected. The second stage is shown in Fig. 2(d) where $\mathbf{t}_0 = \mathbf{s}_1$ was classified after four target signatures $\mathbf{t}_1$, $\mathbf{t}_2$, $\mathbf{t}_3$, $\mathbf{t}_4$ were generated and eliminated subsequently by orthogonal projection. Its corresponding OPCI was reduced to $\eta_4 = 0.00174$. From this image, the panels in rows 1–3 were detected. The third stage occurred in Figs. 2(e)–2(k) after the fifth target signature $\mathbf{t}_5$ was generated and eliminated where the panels in rows 2–3 detected in Fig. 2(d) began to fade away and vanish. The fourth stage was observed by Figs. 2(l)–2(t) where the image background was cleaned up after the 12th target signature $\mathbf{t}_{12}$ was generated and eliminated. Also demonstrated is the change between Fig. 2(p) and 2(q) where panels in rows 2–4 detected in Figs. 2(l)–2(p) were eventually eliminated after the 17th target signature $\mathbf{t}_{17}$ was eliminated. As a matter of fact, as shown in Figs. 2(q)–2(t) very little change was made after elimination of the 17th target signature $\mathbf{t}_{17}$. Such drastic transitions from the first stage to the fourth stage resulted from elimination of the 4th, 5th, and 12th target signatures $\mathbf{t}_4$, $\mathbf{t}_5$, $\mathbf{t}_{12}$, $\mathbf{t}_{17}$. This implies that $\mathbf{t}_4$, $\mathbf{t}_5$, $\mathbf{t}_{12}$, and $\mathbf{t}_{17}$ possess very distinct spectral features. These phenomena are also illustrated by rapid reduction in the values of the OPCI, from $\eta_3 = 0.01807$ to $\eta_4 = 0.00174$, from $\eta_4 = 0.00174$ to $\eta_5 = 0.00114$, $\eta_{11} = 0.00069$ to $\eta_{12} = 0.00026$, $\eta_{16} = 0.00022$ to $\eta_{17} = 0.00018$. It should be noted that the panels in the third column has size of $1\ \mathrm{m} \times 1\ \mathrm{m}$ which is smaller than the 1.5 m pixel resolution. As a result, they cannot be visualized in Fig. 1(b). Interestingly, some of these panel pixels were detected in Figs. 2(l)–2(p). In particular, the panel pixel p_{13} was embedded in a single pixel. It

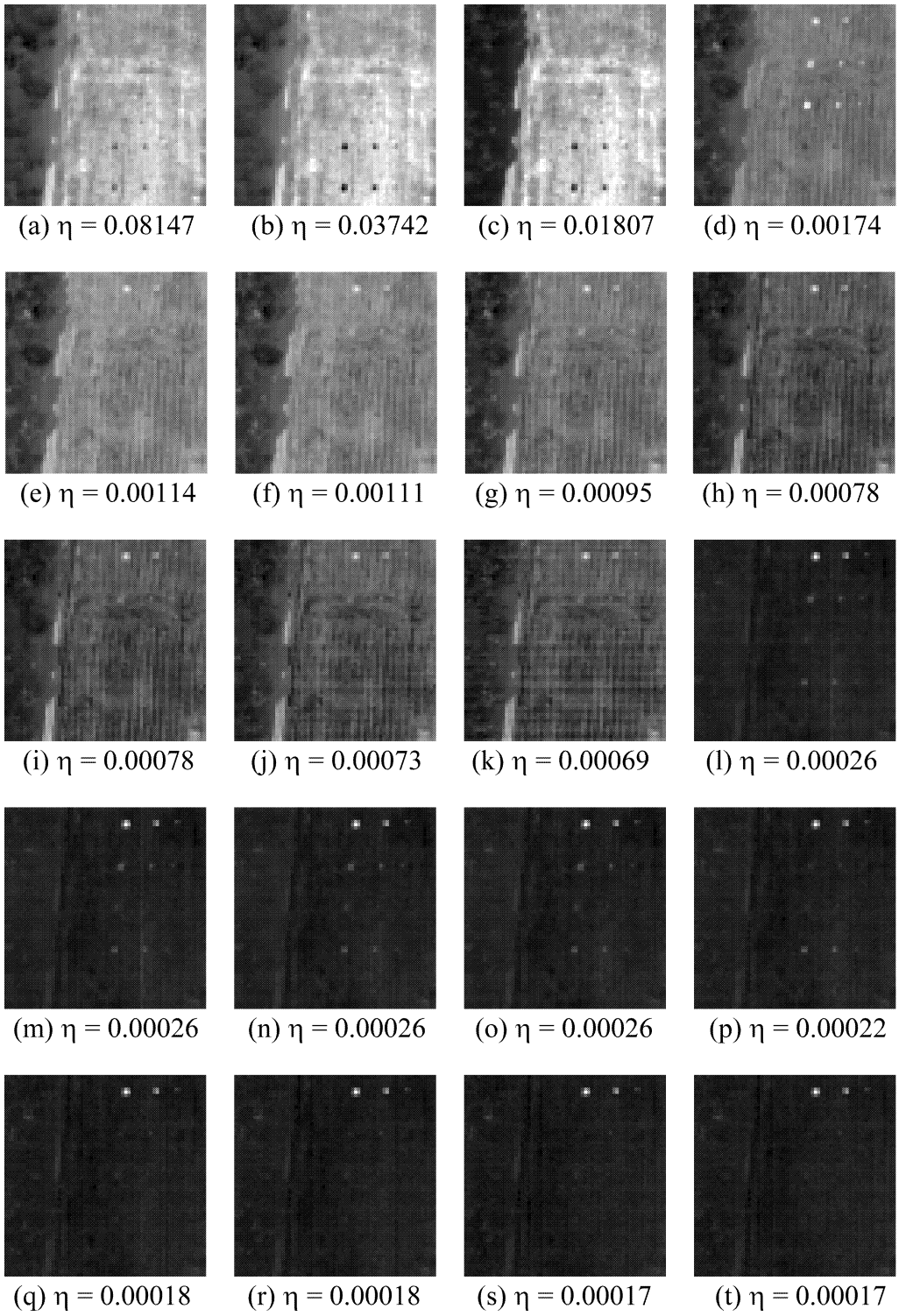

Fig. 2. Results produced by DTDCA using $\mathbf{s}_1$ as initial target signature $\mathbf{t}_0$.

was not shown in Fig. 1(b) but was detected by the DTDCA in Figs. 2(q)–2(t). This further shows that the DTDCA has capability of detecting targets at subpixel level.

Similar experiments were also conducted for detection of panels in rows 2–5 using the panels signatures $\mathbf{s}_2, \mathbf{s}_3, \mathbf{s}_4, \mathbf{s}_5$ as the desired target signatures $\mathbf{t}_0$ for each row. Their classification results are shown in Figs. 3–6 respectively. For the purpose of comparison, the maximum number of target signatures required to generate was set to 20 to terminate the ATGP, which was the same number used for Fig. 2. As shown in these figures, the DTDCA detected panel pixels in each row separately and effectively where the OPCI

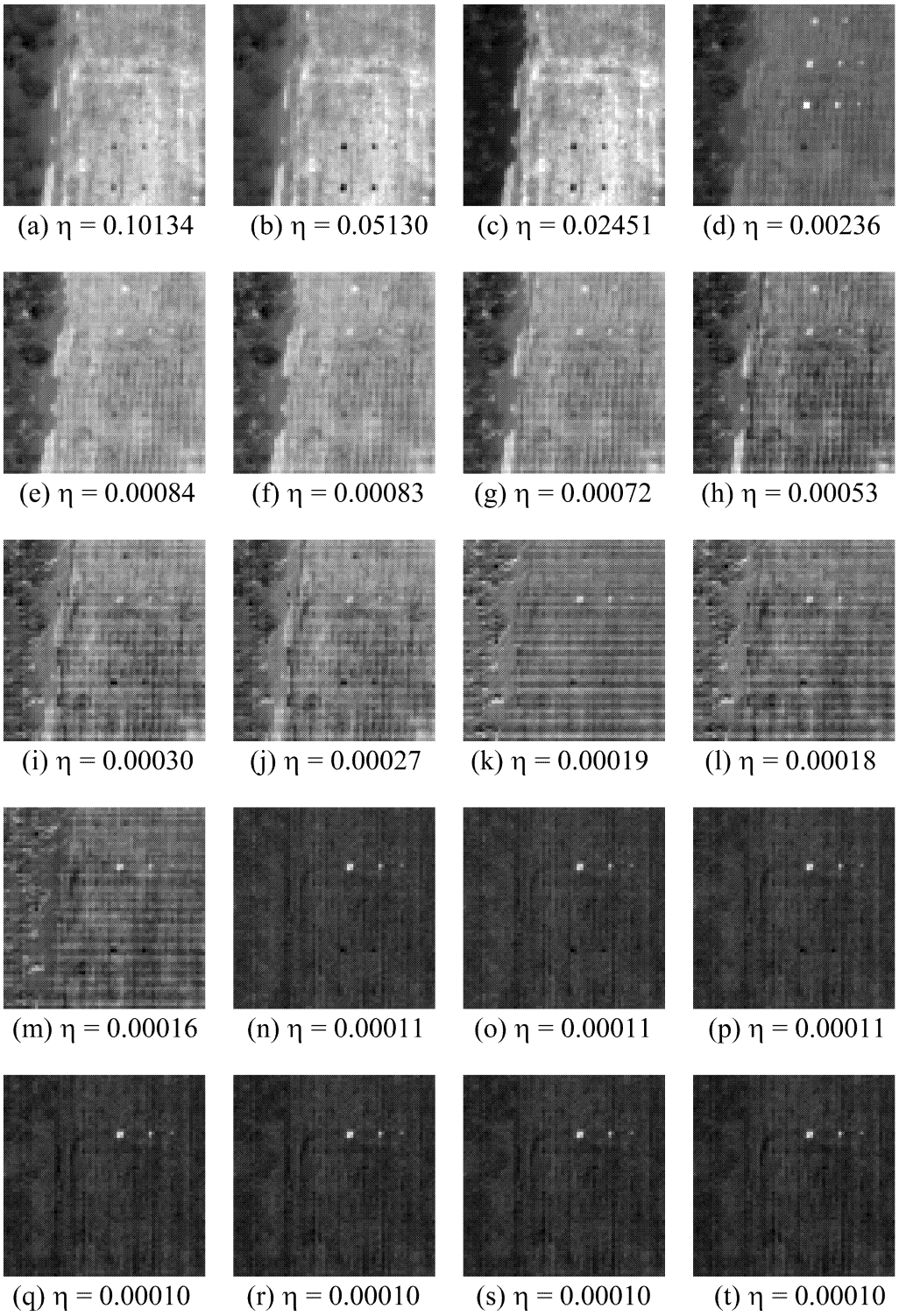

Fig. 3. Results produced by DTDCA using $\mathbf{s}_2$ as initial target signature $\mathbf{t}_0$.

values used to generate 20 target signatures were different.

In order to evaluate the performance of the DTDCA, we compared it to the OSP classifier specified by (6) which was developed in [7, 9]. Two reasons lead us to choosing the OSP classifier as a benchmark comparison. 1) The OSP is a widely used linear unmixing method and has become a standard hyperspectral imaging technique [18]. 2) As shown in [9, 11, 19] the OSP approach was a very general linear unmixing method, which includes the MLC as a special case. Figs. 7(a)–7(e) show results produced by the OSP classifier for classification of panels in rows 1–5, respectively. Since the OSP classifier requires the

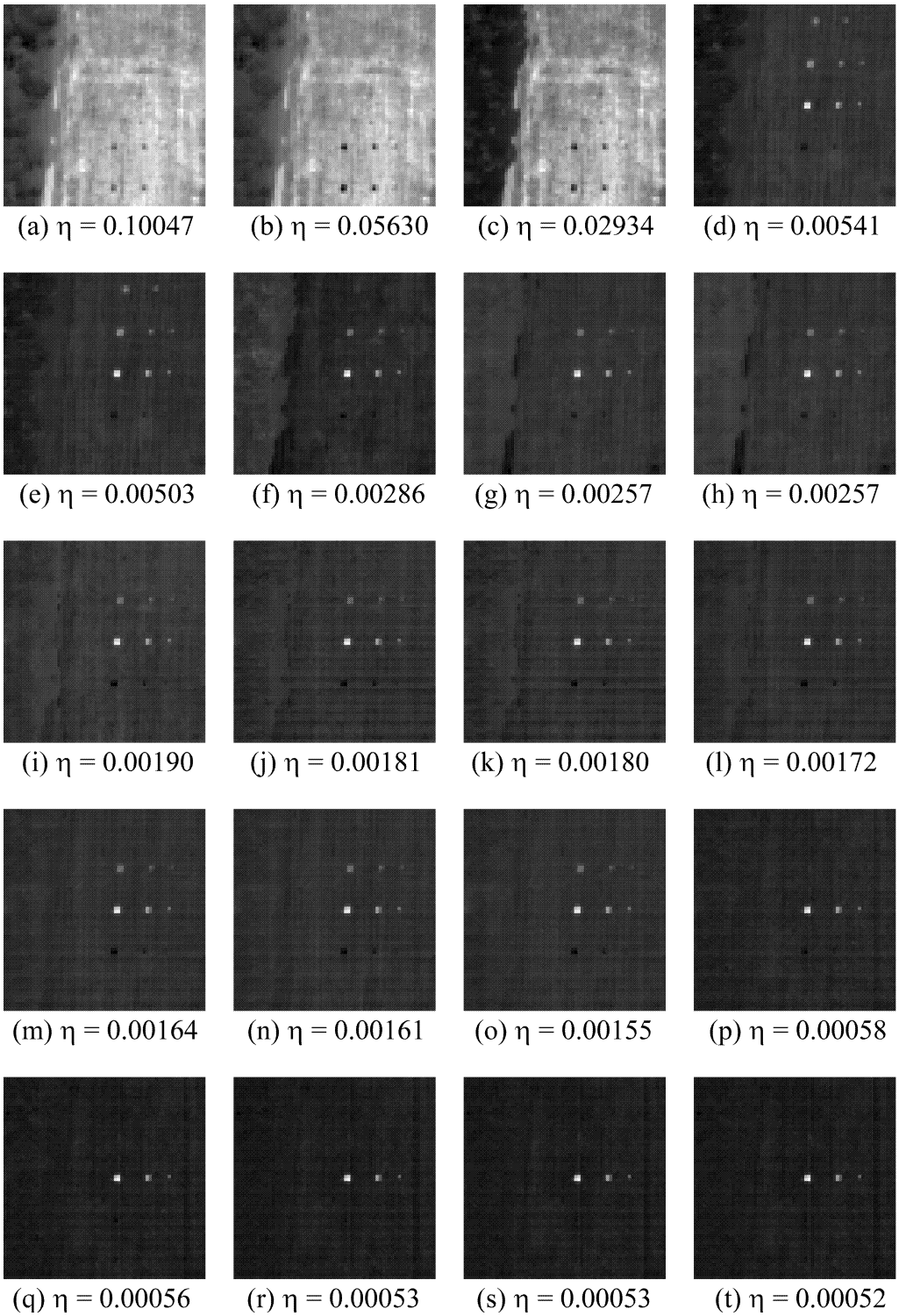

Fig. 4. Results produced by DTDCA using $\mathbf{s}_3$ as initial target signature $\mathbf{t}_0$.

complete knowledge of target signatures present in the image scene, seven target signatures were selected to represent the image scene and to produce Fig. 7. The used seven target signatures were 5 panel signatures, $\{\mathbf{s}_i\}_{i=1}^{5}$ plotted in Fig. 1(d) plus two background signatures, a tree signature and a grass signature selected by visual inspection of the scene. Comparing Fig. 7(a) to Fig. 2(t), Fig. 7(b) to Fig. 3(t), Fig. 7(c) to Fig. 4(t), Fig. 7(d) to Fig. 5(t) and Fig. 7(e) to Fig. 6(t), we can see that the DTDCA performed significantly better than did the OSP classifier because the DTDCA made use of the ATGP to generate 20 undesired target signatures for elimination as opposed to only 6 undesired target signatures used by the OSP

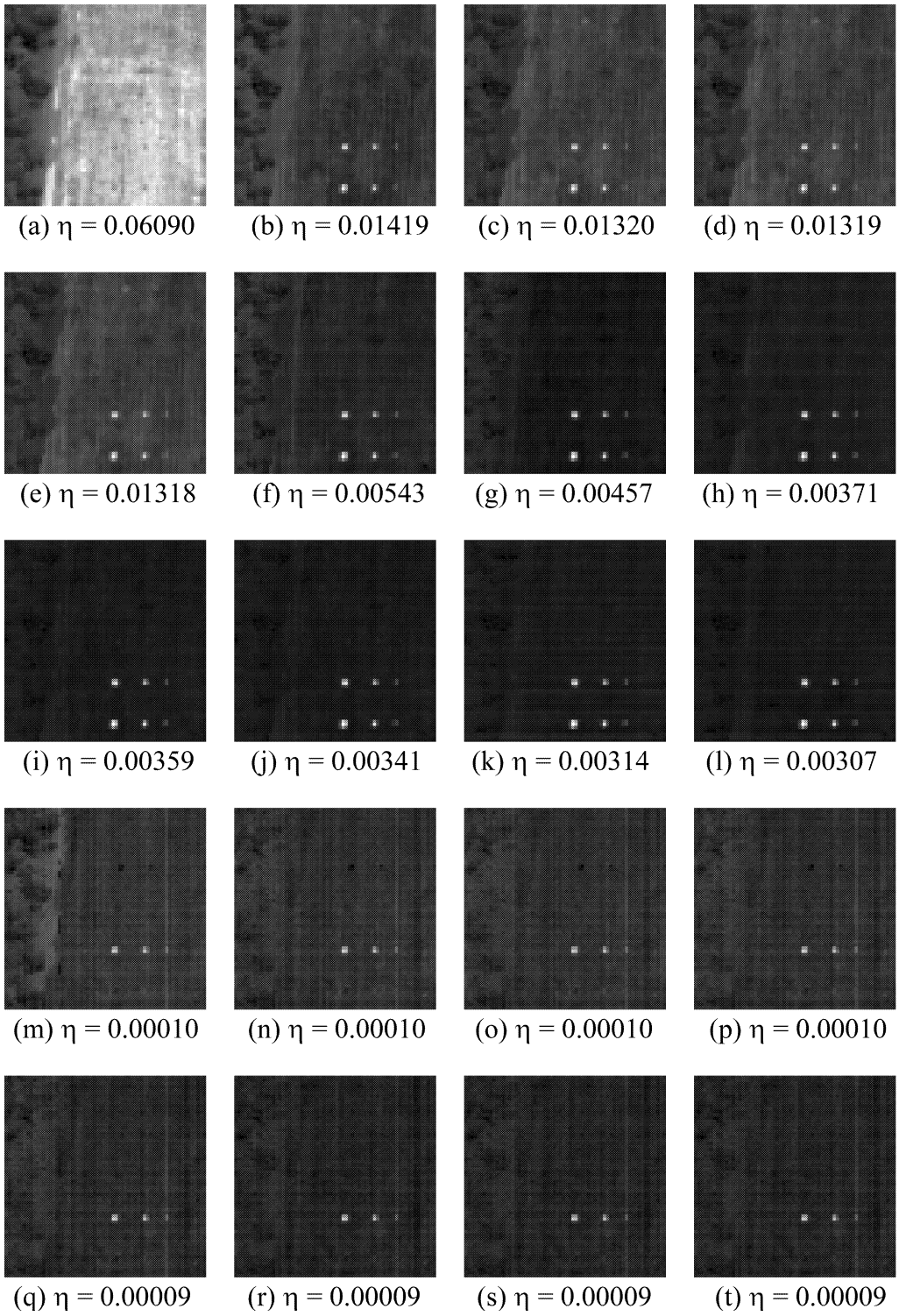

Fig. 5. Results produced by DTDCA using $\mathbf{s}_4$ as initial target signature $\mathbf{t}_0$.

classifier for elimination. However, it should be noted that the OSP made full use of the knowledge of the five panel signatures $\{\mathbf{s}_i\}_{i=1}^{5}$, while the DTDCA only required the knowledge of the desired target signature, $\mathbf{s}_i$ without knowing $\mathbf{s}_j$ for $j \neq i$.

Since the images generated in Figs. 2–6 were actually abundance fractional images of panel pixels which were gray scale, their classification was performed by visual inspection. With the ground truth map provided in Fig. 1(c), we can further conduct quantitative study by tabulating the results of detection and classification of B panel pixels in each row. In order to do so, we need to convert gray scale abundance fractional images to binary images. One such technique was developed in [19], referred to as abundance percentage cut-off thresholding.

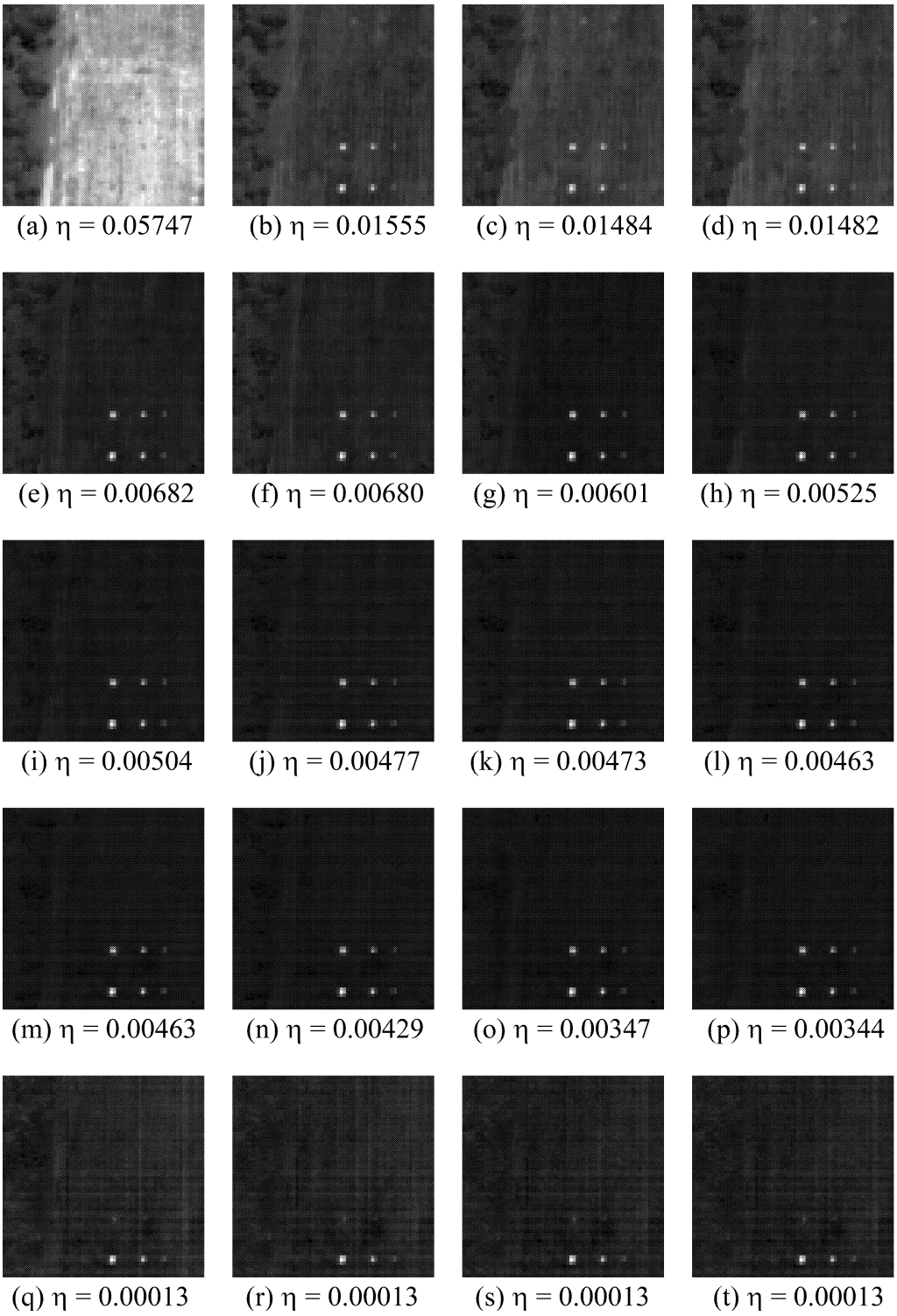

Fig. 6. Results produced by DTDCA using $\mathbf{s}_5$ as initial target signature $\mathbf{t}_0$.

It normalized abundance fractions of each pixel to the range of [0,1], then chose a cut-off abundance percentage $a\%$ as a threshold value. If the abundance fraction of a pixel was greater than or equal to the specified $a\%$ (i.e., $\geq a/100$), the pixel would be declared as a target pixel and be assigned by 1 and those pixels with abundance fractions less than $a\%$, i.e., $< a/100$ would be considered as background pixels and assigned by 0. Using this abundance percentage cut-off thresholding we tabulate the DTDCA results of Figs. 2(t)–6(t) in Table I and the OSP classification results of Figs. 7(a)–7(e) in Table II where $a\%$ was chosen to be 10%, 25%, 50%. In particular,

N = total number of black panel pixels in the scene;
$N_{\mathrm{B}}(i)$ = number of B panel pixels in row i;

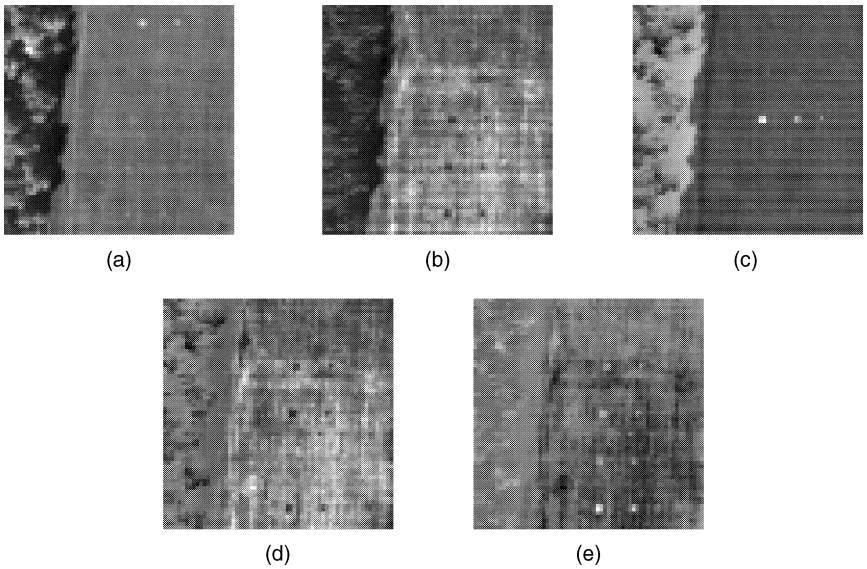

Fig. 7. Results of the OSP classifier. (a) Panels in row 1. (b) Panels in row 2. (c) Panels in row 3. (d) Panels in row 4. (e) Panels in row 5.

TABLE I
Detection Results of DTDCA for B Panel Pixels Using $a\%$ = 10%, 25% and 50%

		a = 10%			a = 25%			a = 50%		
Row	$N_B(i)$	$N_{BD}(i)$	$N_M(i)$	$N_F(i)$	$N_{BD}(i)$	$N_M(i)$	$N_F(i)$	$N_{BD}(i)$	$N_M(i)$	$N_F(i)$
row 1	3	3	0	1036	2	1	1	2	1	0
row 2	4	4	0	3745	4	0	386	4	0	0
row 3	4	4	0	1110	4	0	0	3	1	0
row 4	4	4	0	3730	4	0	26	3	1	0
row 5	4	4	0	2140	3	1	1	3	1	0
Total	19	19	0	11761	17	2	414	15	4	0

TABLE II
Detection Results of OSP for B Panel Pixels Using $a\%$ = 10%, 25% and 50%

Using Background Signatures										
		a = 10%			a = 25%			a = 50%		
Row	$N_B(i)$	$N_{BD}(i)$	$N_M(i)$	$N_F(i)$	$N_{BD}(i)$	$N_M(i)$	$N_F(i)$	$N_{BD}(i)$	$N_M(i)$	$N_F(i)$
row 1	3	3	0	3879	3	0	3441	3	0	297
row 2	4	4	0	3609	4	0	3200	4	0	1446
row 3	4	4	0	4051	4	0	3825	4	0	712
row 4	4	4	0	4046	4	0	3957	4	0	1674
row 5	4	4	0	4049	4	0	3776	3	1	1019
Total	19	19	0	19634	19	0	18199	18	1	5148
Without Using Background Signatures										
		a = 10%			a = 25%			a = 50%		
Row	$N_B(i)$	$N_{BD}(i)$	$N_M(i)$	$N_F(i)$	$N_{BD}(i)$	$N_M(i)$	$N_F(i)$	$N_{BD}(i)$	$N_M(i)$	$N_F(i)$
row 1	3	3	0	3822	3	0	1560	0	3	241
row 2	4	4	0	4046	4	0	4010	4	0	3706
row 3	4	4	0	4030	4	0	3404	3	1	572
row 4	4	4	0	4049	4	0	4042	4	0	3865
row 5	4	4	0	3896	3	0	2511	3	1	181
Total	19	19	0	19843	19	0	15527	14	5	8565

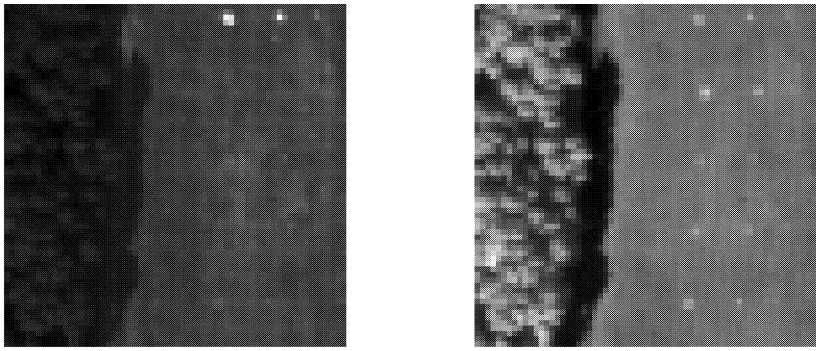

(a) (b)

Fig. 8. Different HYDICE scene from Fig. 1. (a) Band 30. (b) Band 80.

$N_{BD}(i)$ = number of B panel pixels which were detected as B pixels in row i;

$N_F(i)$ = number of false-alarmed B panel pixels in row i, where a false-alarmed B pixel is defined by a non-B pixel which was detected as a B panel pixel;

$N_M(i)$ = number of B panel pixels in row i, which was not detected.

According to Tables I and II, when $a\% = 10\%$, both the DTDCA and the OSP detected all 19 B pixels in all five rows with large numbers of false-alarmed B pixels. As the $a\%$ was increased to 25%, there was little difference in performance for the OSP where all 19 B pixels were detected with a slight reduction of false-alarmed B pixels. By contrast, the DTDCA reduced the total number of false-alarmed B pixels substantially from 11761 to 414 at the expense of missing two B pixels, p_{13} in row 1 and p_{53} in row 5. Specifically, $N_F(2) = 386$ accounted for most of the false-alarmed B pixels with $N_F(1) = N_F(5) = 1$, $N_F(3) = 0$, and $N_F(4) = 26$. If $a\%$ was further increased to 50%, the OSP only missed one B pixel in row 5 while the total number of false-alarmed B pixels was reduced significantly from 18199 to 5148, a two-thirds reduction. Compared with the OSP, the DTDCA missed two more B pixels, p_{33} in row 3 and p_{43} in row 4 with no false-alarmed B pixels, $N_F(i) = 0$ for $i = 1,\ldots,5$. However, if we compare the five detection images in Figs. 2(t)–6(t) produced by the DTDCA to the five detection images in Figs. 7(a)–7(e) produced by the OSP, the DTDCA clearly performed significantly better than the OSP since the gray scale images provide better image interpretation than Tables I and II. Such visual advantage cannot be obtained from quantitative results, which do not show spatial locations of detected pixels and their spatial correlation. For example, the OSP extracted a considerably large number of image background pixels that may obscure a very small number of panel B pixels as shown in Figs. 7(b) and 7(d). Therefore, despite that Tables I–II provide a quantitative analysis of detection results, they do not offer gray level information that is very useful for visual interpretation.

In the above experiments the targets of interest were assumed to be present in the image scene. On some occasions the targets which we are interested may not be in an image scene. In this case, how do we detect their absence in the image scene? The following experiment provides another advantage of the DTDCA which can be used for this purpose.

Fig. 8 is another HYDICE scene similar to that in Fig. 1, which also contains 15 panels in the scene. However, these 15 panels were painted by materials that are different from those used to paint the 15 panels in Fig. 1. Suppose that the targets of interest were panels in row 1 in Fig. 1 and we would like to know if any pixel in Fig. 8 was also painted by the same material that was used to paint the panels in row 1. In this case, we used $\mathbf{s}_1$ as the desired initial target signature $\mathbf{t}_0$ for the scene in Fig. 8. Figs. 8(a)–8(t) show the detection results of applying the DTDCA with $\mathbf{t}_0 = \mathbf{s}_1$ to the scene in Fig. 8 where 20 was set to the maximum number of target signatures required to generate for elimination. As we can see from these figures, the images in Figs. 9(m)–9(t) after elimination of 16 target signatures are completely dark and show no sign of any target pixel whose signature matched $\mathbf{s}_1$. As a consequence, we can conclude that there was no pixel in the image scene in Fig. 8 that was painted by the same material used to paint the panels in row 1 in Fig. 1.

B. Experiments for ATDCA

Unlike the DTDCA, the ATDCA does not assume any prior target knowledge. In this case, the initial target signature $\mathbf{t}_0$ must be generated from the image scene. As a result, it cannot be used to detect targets which are not supposed to be in an image scene as did the DTDCA in Fig. 8.

Additionally, in order to make comparison with the DTDCA, the same image scene used for Figs. 2–6 was also used for the experiments for the ATDCA where the maximum number of target signatures generated by the ATGP was also set to 20. Figs. 10(a)–10(t) show the classification results of the

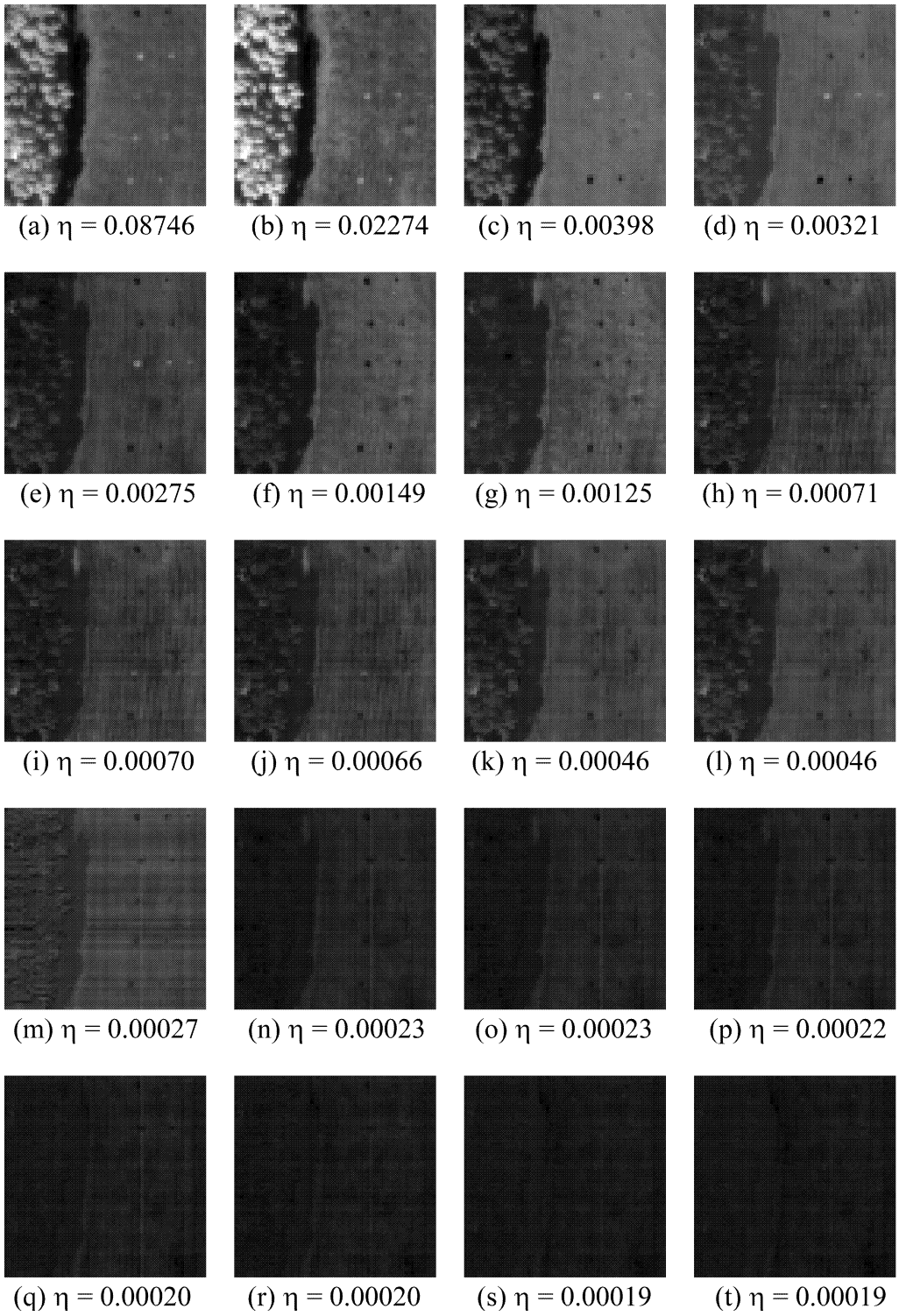

Fig. 9. Results of DTDCA applied to image scene in Fig. 8 when $\mathbf{s}_1$ was used for $\mathbf{t}_0$.

ATDCA where each image was produced by one particular ATGP-generated target signature for detection and classification. Three major differences between the DTDCA and the ATDCA need to be clarified. One is the initial target signatures $\mathbf{t}_0$ used in the ATGP. In the DTDCA the $\mathbf{t}_0$ is the desired target signature and is used as a matching signature for target detection and classification. On the other hand, the initial target signature $\mathbf{t}_0$ in the ATDCA is a target pixel with the maximum vector length, which corresponds to a brightest pixel in an image scene. So, the generated $\mathbf{t}_0$ is not necessarily of our interest. For example, Fig. 10(a) shows the classification of the initial target signature $\mathbf{t}_0$ which was a strong interferer located at the upper left corner. Another difference is that the ATDCA must classify each of

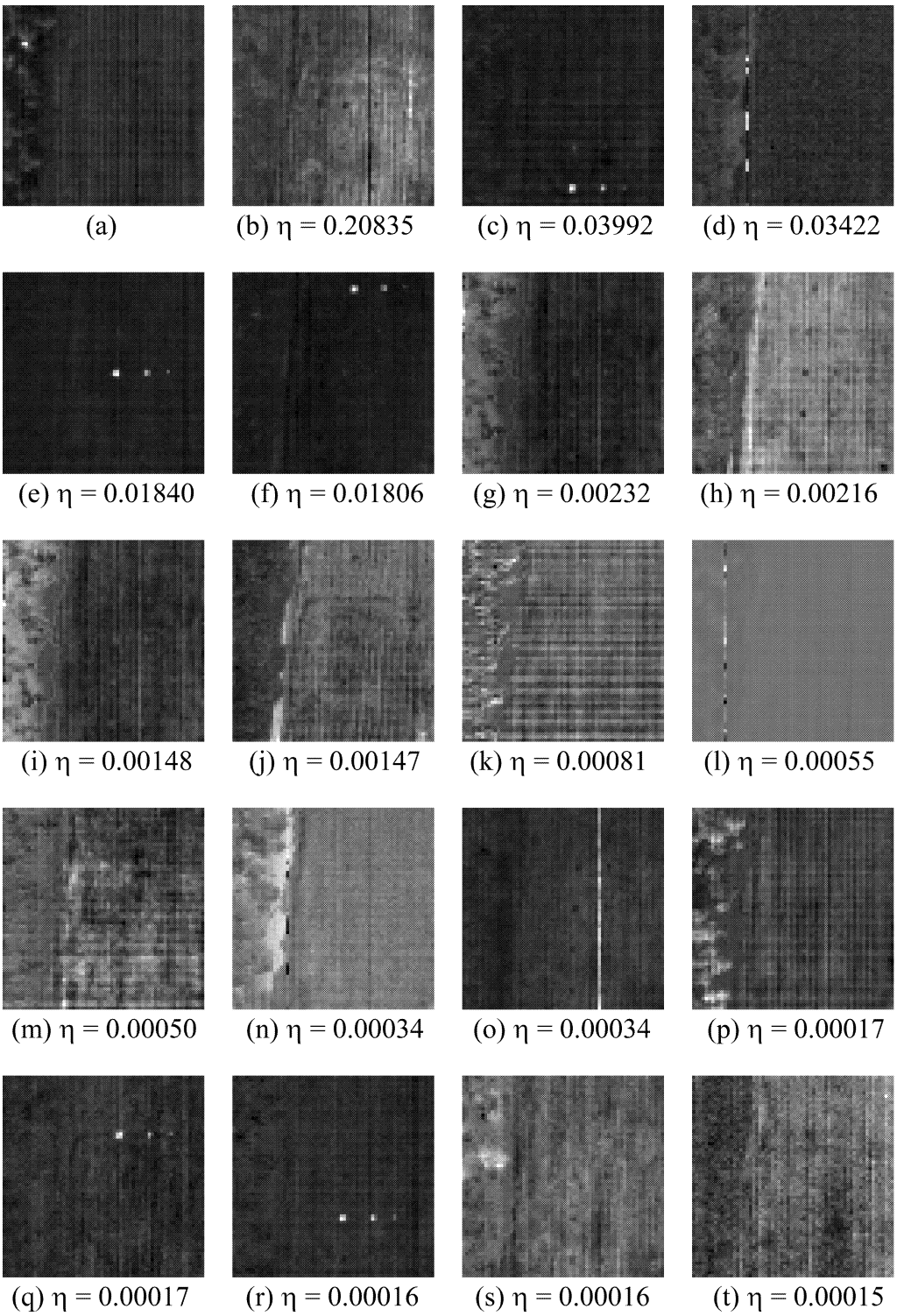

Fig. 10. Results of ATDCA applied to image scene in Fig. 1.

the ATGP-generated target signatures individually and separately. As a result, there were 20 classification images produced by the ATDCA where Figs. 10(c), 10(e), 10(f), 10(q), and 10(r) detected panels in rows 5, 3, 1, 2, and 4, respectively. By contrast, the DTDCA produced only one classification for panels in each row as shown in Figs. 2–6. A third difference is that the 20 target signatures generated by the ATGP in the ATDCA included the initial target signature $\mathbf{t}_0$. This is different from the DTDCA where $\mathbf{t}_0$ was not part of the 20 target signatures generated by the ATGP in the DTDCA. If we compare Figs. 10(c), 10(e), 10(f), 10(q), and 10(r) to Figs. 2(t), 3(t), 4(t), 5(t), and 6(t), there was no visible difference in classification results between the DTDCA and ATDCA.

In analogy with Tables I and II, we can also tabulate the classification results of Figs. 9(c), 9(e), 9(f), 9(q) and 9(r) where the abundance percentage cut-off threshold $a\%$ was also chosen to be 10% and 25%. Interestingly, the results were identical to those in Table 1. These experiments demonstrate that the ATDCA could perform as well as the DTDCA even though the former did not have prior target knowledge as the latter did.

V. CONCLUSION

In this paper, we investigated the problem of ASTR in hyperspectral imagery and developed a two-stage process, ATGP and TCP for the ASTR. The ATGP extracts potential targets directly from image data which may include interferers, unwanted targets, natural background signatures, and clutters. Since hyperspectral images generally contain many unidentified targets in an image scene, the proposed ATGP is particularly attractive in this regard. It overcomes this dilemma and suggests a useful means of extracting potential targets directly from the image scenes without a priori information. Additionally, the proposed ASTR is a versatile technique and can be implemented in two versions, DTDCA and ATDCA to meet various applications. As a matter of fact, one does not necessarily imply another as demonstrated by experiments. For example, the ATDCA can be used for applications such as detection of anomalies and concealed targets in unknown environments [13]. On the contrary, the DTDCA can be used to detect whether a desired target is in the image scene, a task that the ATDCA cannot accomplish as shown in Fig. 9. One intrinsic constraint of the ASTR is that the data dimensionality must be sufficiently large for the ATGP to carry out a sequence of orthogonal projections so that no two target signatures can be accommodated in one dimension, in which case these two targets cannot be distinguished from each other. Apparently, this constraint is not an issue for hyperspectral image data, but it is certainly a problem for multispectral imagery [12, 17]. In order to alleviate this limitation, a generalized OSP method was recently proposed in [17] which can extend the applicability of the ASTR to 3-band SPOT data and Landsat image data for land cover classification rather than target detection and classification.

ACKNOWLEDGMENT

The work of the first author was performed while he was holding a National Research Council Research Associateship Award at Edgewood Chemical and Biological Center, U.S. Army.

REFERENCES

[1] Brumbley, C., and Chang, C.-I (1999)
An unsupervised vector quantization-based target signature subspace projection approach to classification and detection in unknown background.
Pattern Recognition, **32-7** (1999), 1161–1174.

[2] Fukunaga, K. (1990)
Introduction to Statistical Pattern Recognition (2nd ed.).
New York: Academic Press, 1990, ch. 11.

[3] Akaike, H. (1974)
A new look at statistical model identification.
IEEE Transactions on Automatic Control, **19** (1974), 716–723.

[4] Wax, M., and Kailath, T. (1985)
Detection of signals by information theoretic criteria.
IEEE Transactions on Acoustics, Speech and Signal Processing, **33** (1985), 387–392.

[5] Rissnan, J. (1978)
Modelling by shortest data description.
Automatica, **14** (1978), 465–471.

[6] Chang, C.-I (2003)
Hyperspectral Imaging: Techniques for Spectral Detection and Classification.
New York: Kluwer Academic Publishers, 2003.

[7] Harsanyi, J. C., and Chang, C.-I (1994)
Hyperspectral image classification and dimensionality reduction: An orthogonal subspace projection.
IEEE Transactions on Geoscience and Remote Sensing, **32** (1994), 779–785.

[8] Chang, C.-I, Sun, T-L., and Althouse, M. L. G. (1998)
An unsupervised interference rejection approach to target detection and classification for hyperspectral imagery.
Optical Engineering, **37** (1998), 735–743.

[9] Chang, C.-I, Zhao, X., Althouse, M. L. G., and Pan, J-J. (1998)
Least squares subspace projection approach to mixed pixel classification in hyperspectral images.
IEEE Transactions on Geoscience and Remote Sensing, **36** (1998), 879–892.

[10] Settle, J. J. (1996)
On the relationship between spectral unmixing and subspace projection.
IEEE Transactions on Geoscience and Remote Sensing, **34** (1996), 1045–1046.

[11] Chang, C.-I (1998)
Further results on relationship between spectral unmixing and subspace projection.
IEEE Transactions on Geoscience and Remote Sensing, **36** (1998), 1030–1032.

[12] Chang, C.-I, and Brumbley, C. (1999)
Linear unmixing Kalman filtering approach to signature abundance detection, signature estimation and subpixel classification for remotely sensed images.
IEEE Transactions Aerospace and Electronic Systems, **37** (1999), 319–330.

[13] Ren, H., and Chang, C.-I (1998)
A computer-aided detection and classification method for concealed targets in hyperspectral imagery.
In *Proceedings of International Symposium on Geoscience and Remote Sensing '98*, Seattle, WA, July 5–10, 1998, 1016–1018.

[14] Adams, J. B., Smith, M. O., and Gillespie, A. R. (1993)
Image spectroscopy: Interpretation based on spectral mixture analysis.
In *Remote Geochemical Analysis: Elemental and Mineralogical Composition*, C. M. Pieters and P. A. Englert (Eds.), New York: Cambridge University Press, 1993, 145–166.

[15] Settle, J. J., and Drake, N. A. (1993)
Linear mixing and estimation of ground cover proportions.
International Journal of Remote Sensing, **14** (1993), 1159–1177.

[16] Special Issue on Hyperspectral Analysis and Applications.
IEEE Transactions on Geoscience and Remote Sensing, **39** (2001).

[17] Ren, H., and Chang, C.-I (2000)
A generalized orthogonal subspace projection approach to unsupervised multispectral image classification.
IEEE Transactions on Geoscience and Remote Sensing, **38** (2000), 2515–2528.

[18] Schwengerdt, R. A. (1997)
Remote Sensing: Models and Methods for Image Processing (2nd ed.).
San Diego, CA: Academic Press, 1997, 470–471.

[19] Ren, H., and Chang, C.-I (2000)
An experiment-based quantitative and comparative analysis of hyperspectral target detection and image classification algorithms.
IEEE Transactions on Geoscience and Remote Sensing, **38** (2000), 1044–1063.

Hsuan Ren (S'98—M'00) received the B.S. degree in electrical engineering from the National Taiwan University, Taipei, Taiwan, R.O.C., in 1994 and the M.S. and Ph.D. degrees from Unicersity of Maryland Baltimore County in 1998 and 2000, respectively, all in electrical engineering.

He received a National Research Council (NRC) Research Associateship award supported by U.S. Army Edgewood Chemical Biological Center from 2000 to 2003. He is current an assistant professor in National Central University, Chung-Li, Taiwan, R.O.C. His research interests include data compression, signal and image processing and pattern recognition.

Dr. Ren has two patents pending on hyperspectral target detection and image classification. He is a member of SPIE and of the honor society of Phi Kappa Phi.

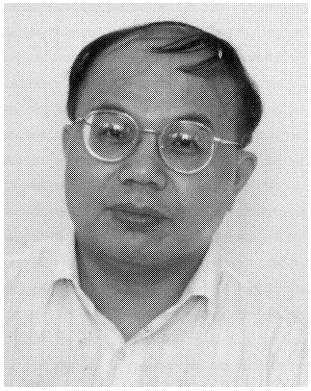

Chein-I Chang (S'81—M'87—SM'92) received the B.S. degree from Soochow University, Taipei, Taiwan, 1973, the M.S. degree from the Institute of Mathematics at National Tsing Hua University, Hsinchu, Taiwan, in 1975 and the M.A. degree from the State University of New York at Stony Brook, in 1977, all in mathematics. He also received the M.S. and M.S.E.E. degrees from the University of Illinois at Urbana–Champaign, in 1982, and the Ph.D. degree in electrical engineering from the University of Maryland, College Park, in 1987.

Dr. Chang has been with the University of Maryland Baltimore County (UMBC) since 1987, as a visiting assistant professor from January 1987 to August 1987, assistant professor from 1987 to 1993, associate professor from 1993–2001 and professor in the Department of Computer Science and Electrical Engineering since 2001. He was a visiting research specialist in the Institute of Information Engineering at the National Cheng Kung University, Tainan, Taiwan, from 1994–1995. He received an NRC (National Research Council) senior research associateship award from 2002–2003 at the U.S. Army Soldier and Biological Chemical Command, Edgewood Chemical and Biological Center, Aberdeen Proving Ground, MD. His research interests include automatic target recognition, multispectral/hyperspectral image processing, medical imaging, information theory and coding, signal detection and estimation, neural networks.

Dr. Chang has a patent on automatic pattern recognition and several pending patents on image processing techniques for hyperspectral imaging and detection of microcalcifications. He is on the editorial board and was the guest editor of a special issue on telemedicine and applications of the *Journal of High Speed Networks*. He authored a book, *Hyperspectral Imaging: Techniques for Spectral Detection and Classification* published by Kluwer Academic Publishers. Dr. Chang is an associate editor in the area of hyperspectral signal processing for *IEEE Transactions on Geoscience and Remote Sensing* and a Fellow of SPIE and a member of Phi Kappa Phi and Eta Kappa Nu.